

Chapter 3

Chapter 3 : Structure factor, Energy loss and Wake effects in Gapped Graphene

We report our theoretical investigation on Structure factor, Energy loss and wake effects in gapped graphene. The Gap in a SLG is introduced by introducing a mass term Δ , which breaks the sublattice symmetry. The model consists of a single layer gapped graphene lying on SiO_2 substrate. The calculations are carried within RPA density-density response function. Since $\chi(q, \omega)$ is linearly proportional to q at large q and decreases only like ω^{-1} at large ω in both gapped and gapless graphene, accordingly the structure factor obtained is divergent. In order to improve divergence, we need to add and subtract vacuum polarization inside frequency integral and regularize the structure factor for gapped graphene as well. . We also evaluated dynamic and static structure factor of gapped graphene, numerically. The values of structure factor were used to obtain numerical results for energy loss. An external particle is moving above this gapped graphene sheet at a height H , which has a range in \AA . We study here the energy loss occurring due to interaction between particle and the sheet. The analytical solution of energy loss comes out to be in terms of Bessel function. It is found that the energy loss reduces on increasing the value of gap and particle velocity increases the magnitude of energy loss reduces. As velocity of particle increases it has got less time to interact with the system resulting into less energy loss. The increase in the value of coupling constant also increases the magnitude of energy loss. Wake effect is the disturbance caused in a medium by moving external particle or an object in motion, outside or inside the medium. The charge induced by this external charge can be calculated using an appropriate methodology. The visible example of wake effect is wake oscillations created by a travelling boat in a sea with the waves trailing behind the boat. This chapter reports

analytical as well as numerical calculations on wake effects in gapped graphene. The results are quite unique with oscillations being observed leading the particle as well similar to past results obtained for carbon nanotubes. The infinite upper limit, for q integration, has solution in terms of Whittaker function. With a finite cut-off the number of waves and amplitude reduces.

3.1 Introduction

Because of its unique features, Graphene has been immensely studied in recent years [1-3]. Its unique properties have developed it as a promising material for technological applications. With significant rise in the research and its application in industries, the modification in the substance is also being considered by scientists and researchers across the world. One of it is introducing a gap in between valence and conduction band through various techniques e.g. Spin-Orbit Interaction, Breaking of Sublattice symmetry, External magnetic Field, Finite geometry effect and various other instabilities. The dispersion relation of gapped graphene differs from that of SLG by a value Δ i.e. $E(\mathbf{k}) = \sqrt{\hbar^2 v_f^2 k^2 + \Delta^2}$ [4]. Gapped Graphene can be considered a substitute to 2DEG semiconductor material. Devices based on gapped graphene have better working efficiency compared to the semiconductor devices because of change in electronic properties. A gap can also be introduced in graphene by radiating it with circularly polarized electric field, where the gap can be varied and maintained by tuning the frequency and intensity of the light. Theoretically the model was developed by Roslyak and group [5]. They have calculated the Hamiltonian for dressed Dirac electrons in presence of circularly polarized electric field and used those results to obtain the noninteracting polarization function and plasmons within RPA. Another group has obtained

stationary solutions for the electron-photon Dirac equation to describe interaction between graphene and circularly polarized light (CPL) [6]. Moreover the effect of CPL has also been studied by Godfrey Gumbs and group [7], where they have focused on the Plasmon contribution towards the stopping power for graphene and double layer graphene numerically. They have compared the Plasmon in graphene and gapped graphene. Experimentally, a gap in between the conduction and valence band in graphene can be introduced by various well known techniques. It can be done by substrate induced techniques, spin orbit interactions, doping, absorption of water molecules, applying gate voltage, confinement of dimensions (dot, nanoribbons), hybrids, Kekule lattice distortion etc. All these techniques can create a gap of approximately 10^{-3} eV upto 0.5 eV.

Fazel Yavari and group [8] has shown that a gap up to ≈ 0.2 eV can be obtained by adsorption of water molecules on graphene sheet and have observed that this effect is reversible i.e. the gap reduces up to ≈ 0.029 eV when the humidity is almost zero. Extensive research has been carried out to obtain Graphene Nanoribbons (GNRs) since the discovery that it can be used as a principal material in devising FETs (Field effect Transistor). Various techniques have been reported in literature [9] to obtain the GNRs such as patterning and etching, catalytic nanocutting of graphene, SPM based lithography, unzipping of carbon nanotubes etc. A gap can also be created by applying an external magnetic field [10].

Resa Asgari and group [11] has reviewed several literatures and listed in brief several scenarios to open a gap in the band energy structure of graphene, such as finite size effect in graphene nanoribbons, zigzag shaped edges where the band arises from a staggered sublattice potential due to magnetization at the edge, doping with chemical species, interaction of graphene with CrO_3 molecules generating a gap of

about 0.12 eV at the Dirac point, placing graphene on SiC substrate or hexagonal Boron nitride which breaks the sublattice symmetry generating a gap of 0.26eV and 53 meV respectively, applying the magnetic field. The other mechanism listed in the paper are electrons hopping on a honeycomb lattice with textured tight-binding hopping amplitudes, the Kekul'e texture, generates a Dirac gap, spin-orbit coupling or Rashba effect.

ARPES is used to prove experimentally the band structure of graphene or gapped graphene. ARPES, also known as ARUPS (angle-resolved ultraviolet photoemission spectroscopy), is a direct experimental technique to observe the distribution of the electrons (more precisely, the density of single-particle electronic excitations) in the reciprocal space of solids. ARPES is one of the most direct methods of studying the electronic structure of the surface of solids. ARPES gives information on the direction, speed and scattering process of valence electrons in the sample being studied (usually a solid). This means that information can be gained on both the energy and momentum of an electron, resulting in detailed information on band dispersion and Fermi surface. This technique is a refinement of ordinary photoemission spectroscopy [12].

3.1.1 Structure Factor and Energy loss

Structure factor of SLG has been discussed in detail in chapter 2. We compare structure factor of gapped graphene with that of SLG in this chapter. The structure factor provides a medium to calculate various important quantities of the system, one such important property being energy loss. The relation between dynamic structure factor and energy loss is given by eq. 1.18 in chapter 1.

Electron energy loss spectroscopy/High resolution Electron energy loss spectroscopy (EELS/HREELS) :

The amount of energy loss can be measured experimentally through EELS. In this process a beam of electron is incident on the surface of the substance. The electrons undergo inelastic scattering and lose some amount of energy and deflect their original path. The EELS helps in probing the surface properties of the substance. Inelastic interactions include phonon excitations, inter and intra-band transitions, [plasmon](#) excitations, inner shell ionizations, and [Čerenkov](#) radiation. However a more precise experimental method for low energy incident beam of electrons (~ 10 eV) would be High Resolution Electron Energy Loss Spectroscopy (HREELS). It is highly surface sensitive and best suited when the energy of incident electrons is low [13].

In an electron energy loss study of surface vibrations, the sample is placed in ultrahigh vacuum. A highly monoenergetic beam of electrons is directed toward the surface, and the energy spectrum and angular distribution of electrons backscattered from the surface are measured. In a typical experiment, the kinetic energy of the incident electrons is in the range of a few electron volts. Detailed information on experimental setup is provided in link mentioned in reference [14].

The contribution of Plasmons in energy loss in graphene have been studied experimentally by scanning tunneling microscopy (STEM) EELS [15-17].

In recent years several research groups have carried out work on gapped graphene both experimentally and theoretically. Quantities such as dynamical polarization, screening and plasmons have been studied at $T=0$ K by Pyatkovskiy [4]. Polarization and stopping and image forces have also been studied by I.Radovic and group [18]. They have also included effect of temperature. Stopping and image forces have also been studied for graphene on SiO_2 substrate, under the gating conditions. Spectrum of gapped graphene has been discussed by kumar gupta and

group [19], while Ground state properties such as exchange correlation and ground state energies and compressibility were calculated by Alireza and Resa Asgari [11]. Electronic structure of gapped graphene has been discussed by Wei Zhu and group [20].

Power loss of an energetic charged particle moving parallel to graphene sheet has been previously studied for SLG [21]. Energy loss has been reported by Godfrey gumbs and group, they have compared stopping power of graphene layer and double layer in presence and absence of gap. Mainly they have shown results with varying particle velocity. Structure factor basically describes the structure of system being considered. It has been previously reported for 2DEG [22], Bilayer Graphene [23].

3.1.2 Wake-effects

Wake potential is produced by a charged particle moving in a medium, and which appears behind in the region already traversed by the particle (in its "wake") due to the medium polarization. The corresponding electric charge is referred to as the wake charge. The emergence of the wake potential affects the passage of a beam of charged particles through a medium, since each particle is acted upon by the wake potential generated by preceding particles. Oscillations of the wake charge density result in an additional ionization added to that directly produced by the charged particle. This secondary ionization proceeds along the whole track axis for a certain period of time after the particle has passed, but it has retarded with respect to primary ionization. Because of the wake potential the track of a charged particle appears to be linear source of secondary electrons. The difference between the dielectric constant in the particle track and that of the surrounding space or medium results in the Raman scattering of light from the wake charge oscillations [24].

Light scattering due to surface wakes has been studied theoretically by I. Kamohara and Y. H. Ohtsuki. It is shown that soft X-rays scattered by surface wake present very characteristic angular and energy distribution. The detectability of this effect is estimated in the case of synchrotron radiation [25].

The energy loss and wake effects are important physical quantities that are required to be studied at zero temperature to understand response of the system. The wake effects have been reported numerically till now, for graphene, and lacked the analytical support for the system while energy loss has been reported in a simplified manner for graphene [21] and gapped graphene [7]. Though analytical results were missing for later case. This chapter reports analytical and numerical solutions of energy loss and wake effects of gapped graphene. Numerical results for dynamic and static structure factor have also been reported. This chapter is organized as follows. Formalism has been reported in section 3.2 followed by results and discussion in section 3.3. The references are quoted in section 3.4

3.2 Formalism

3.2.1 Structure Factor and Energy loss

The Structure factor for gapped graphene can be calculated using the formalism used in chapter 2. The dynamic structure factor can be used to obtain energy loss of the system.

We study the energy loss of energetic charged particle moving parallel to gapped graphene sheet in the x -direction at height H above x - y plane ($z=0$) with velocity v and charge number Z . The formalism for energy loss already exists in literature [26] but it is stated below briefly for review.

The screening of function $K(1,2)$ due to potential $U(2)$ at point $2 = (\vec{r}_2, t_2)$ results in effective potential $V(1)$ at space time point $1 = (\vec{r}_1, t_1)$

$$V(1) = \int d^4 2 K(1,2)U(2) \quad (3.1)$$

Where K is the space-time matrix inverse of the dielectric function ϵ , such that

$$\int d^4 3 K(1,3) \epsilon(3,2) = \int d^4 3 K(3,2) \epsilon(1,3) = \delta^4(1,2) \quad (3.2)$$

Including density perturbation involved in the response dynamics

$$\rho(1) = \int d^4 3 R(1,3)V(3) \quad (3.3)$$

$$= \int d^4 3 \int d^4 4 R(1,3)K(3,4)U(4) \quad (3.4)$$

$R(1,3)$ being the density perturbation response function

The 2D fourier transform yields

$$\vec{r}_1 - \vec{r}_2 \rightarrow \vec{q} \text{ and } t_1 - t_2 \rightarrow \omega$$

$$\int dz_2 K(\vec{q}, z_1, z_2; \omega) \epsilon(\vec{q}, z_2, z_3; \omega) = \delta(z, z_3) \quad (3.5)$$

$$K(\vec{q}, z_1, z_2; \omega) = \frac{1}{\epsilon_0} \delta(z_1 - z_2) + \frac{1}{\epsilon_0} \delta(z_2) e^{-q|z_1|} [K^{2D}(\vec{q}, \omega) - 1] \quad (3.6)$$

Where

$$K^{2D}(\vec{q}, \omega) = [1 + \frac{\alpha^{2D}(\vec{q}, \omega)}{\epsilon_0}]^{-1} \quad (3.7)$$

$$= [\epsilon^{2D}(\vec{q}, \omega)]^{-1} \quad (3.8)$$

ϵ^{2D} is the dielectric function defined by eq. 1.19 on the plane and α^{2D} is the polarization.

RPA integral equation yields

$$K(1,2) = \delta^4(1-2) - \int d^43 \alpha(1,3)K(3,2) \quad (3.9)$$

$$\alpha(1,3) = - \int d^44 V_c(1-4)R(4,3) + a_0\delta^4(1-3) \quad (3.10)$$

$$K(1,2) = \frac{1}{\epsilon}\delta^4(1-2) + \frac{1}{\epsilon} \int d^43 \int d^44 V_c(1-4)R(4,3) K(3,2) \quad (3.11)$$

and consequently

$$\nabla_1^2 \left[K(1,2) - \frac{1}{\epsilon}\delta^4(1-2) \right] = -\frac{4\pi e}{\epsilon_0} \int d^43 R(1,3)K(3,2) \quad (3.12)$$

$$\rho(1) = \frac{\epsilon}{4\pi e} \int d^44 \nabla_1^2 \left[K(1,2) - \frac{1}{\epsilon}\delta^4(1-2) \right] U(4) \quad (3.13)$$

Force on an element of Plasma is

$$f = e \int d^31 \rho(1) \vec{\nabla}_1 V(1) \quad (3.14)$$

Rate at which fast particle loses energy is

$$\vec{f} \cdot \vec{v} = v f_x \quad (3.15)$$

Fast particle has a form

$$U(2) = Ze |\vec{r}_2 - Vt_2\hat{i} - H\hat{k}|^{-1} \quad (3.16)$$

$$\therefore \frac{dW}{dt} = \vec{f} \cdot \vec{v} = -\frac{Ze^2v}{2\pi} \int d^2\vec{q} i \frac{q_x}{q} \tilde{K}^{2D}(\vec{q}, -\vec{q} \cdot \vec{v}) [\tilde{K}^{2D}(\vec{q}, -\vec{q} \cdot \vec{v}) - 1] e^{-2qH} \quad (3.17)$$

$$\frac{dW}{dt} = -\frac{Ze^2v}{2\pi} \int d^2\vec{q} e^{-2qH} \frac{q_x}{q} \text{Im} \tilde{K}^{2D}(\vec{q}, -\vec{q} \cdot \vec{v}) \quad (3.18)$$

Above equation can still be further reduced to

$$(\tilde{K}^{2D})^{-1} = \epsilon^{2D} = \epsilon_1^{2D} + i\epsilon_2^{2D} \quad (3.19)$$

$$\epsilon^{2D} = 1 + \alpha^{2D}(\vec{q}, \omega) = 1 - V_{\vec{q}} \chi(\vec{q}, \omega) \quad (3.20)$$

$$\epsilon^{2D} = 1 + \alpha_1^{2D}(\vec{q}, \omega) + i\alpha_2^{2D}(\vec{q}, \omega) \quad (3.21)$$

Energy loss $\frac{dW}{dt}$ in low velocity limit can be stated as

$$\frac{dW}{dt} = -\frac{Z^2 e^2 v^2}{2\epsilon_0} \int d^2\vec{q} e^{-2qH} \frac{q_x^2}{q} \text{Im} \left[\frac{\partial \tilde{K}^{2D}}{\partial \omega}(\vec{q}, \omega = 0) \right] \quad (3.22)$$

$$= -\frac{Z^2 e^2 v^2}{2\epsilon_0} \int dq e^{-2qH} q^2 \left[\frac{\frac{\partial}{\partial \omega} \alpha_2^{2D}(\vec{q}, \omega = 0)}{[\mathcal{E}_1^{2D}(\vec{q}, \omega = 0)]^2} \right] \quad (3.23)$$

In the high velocity limit the energy loss for gapped graphene is evaluated using formalism used by Vassilios Fessatidis and group [21] for obtaining energy loss of SLG.

The polarization function for small energies and momenta can be written as [4]

$$\chi(q, \omega) = \frac{e^2 N_f q^2 \mu}{\epsilon_0 \hbar^2 \omega^2} \left(1 - \frac{\Delta^2}{\mu^2} \right) \quad (3.24)$$

The dielectric function is given as

$$\epsilon(0, \omega) = 1 - \frac{\omega_p^2}{\omega^2} \quad (3.25)$$

Where $\omega_p = \lambda \sqrt{q}$ with $\lambda = \left(\frac{e^2 N_f v_f \sqrt{n\pi}}{\epsilon_0 \hbar \sqrt{1+b^2}} \right)^{\frac{1}{2}}$. The value differs from 2D Plasma in

terms of n and the gap dependence term from SLG.

$$\tilde{K}^{2D}(0, -\vec{q} \cdot \vec{v}) = - \left[1 - \frac{\lambda^2 q}{(\omega + i\eta)^2} \right]^{-1}_{\omega=q_x v} \quad (3.26)$$

where η is the damping parameter

$$\begin{aligned} (\omega + i\eta)^2 &= \omega^2 + 2i\omega\eta + (i\eta)^2 \\ &\cong \omega^2 + i\eta' \end{aligned} \quad (3.27)$$

for $\eta \rightarrow 0$

$$Im\tilde{K}^{2D}(0, -\vec{q} \cdot \vec{v}) = - \left[1 - \frac{\lambda^2 q}{\omega^2 + i\eta'} \right]^{-1}_{\omega=q_x v} \quad (3.28)$$

$$= Im \left[\frac{\omega^2}{\omega^2 - \lambda^2 q + i\eta'} \right] \quad (3.29)$$

$$= \frac{-i}{\pi} \delta \left(1 - \frac{\lambda^2 q}{\omega^2} \right) \quad (3.30)$$

$$\frac{1}{z - z_0 + i\eta} = \frac{-i}{\pi} \delta(z - z_0) \quad (3.31)$$

In general, using the above property of delta function eq. (3.30) can be written

as

Substituting in equ (3.18) we have

$$\frac{dW}{dt} = \frac{2Z^2 e^2 v^2}{\epsilon_0} \int_0^\infty q dq e^{-2qH} \int_0^{\frac{\pi}{2}} d\theta \text{Cos}\theta \delta \left(1 - \frac{\lambda^2}{v^2 q \text{Cos}^2 \theta} \right) \quad (3.32)$$

Executing θ integral

$$\frac{dW}{dt} = -\frac{Z^2 e^2 v^2}{2\epsilon_0 v} \frac{\partial}{\partial H} \left\{ \int_{\frac{\lambda^2}{v^2}}^{\infty} dq e^{-2qH} \left[q \left(q - \frac{\lambda^2}{v^2} \right) \right]^{\frac{-1}{2}} \right\} \quad (3.33)$$

Numerically the energy loss function for gapped graphene can be evaluated by following equation [7]

$$\frac{dW}{dt} = \frac{2 Z^2 e^2 v^2}{\pi} \int_0^{q_{max}} q dq e^{-2qH} \int_0^1 dl \frac{l}{\sqrt{1-l^2}} \text{Im} \left[\frac{1}{\epsilon(q, \omega)} \right] \quad (3.34)$$

where $\text{Im} \left[\frac{1}{\epsilon(q, \omega)} \right] = \frac{\epsilon_2^{2D}(q, qvl)}{[\epsilon_1^{2D}(q, qvl)]^2 + [\epsilon_2^{2D}(q, qvl)]^2}$ is the dynamic structure factor of

gapped graphene and $l = \text{Cos}\theta$

Analytically the Energy loss function has been evaluated for high velocity limit (in 2D Polar coordinates)

The density of states for the gapped graphene

is $D(E_f) = D^0(E_f) \left(\sqrt{1 + \Delta^2/E_f^2} \right) \theta(E_f)$, where $D^0(\epsilon_F) = \frac{g_s g_v E_f}{\pi \hbar^2 v_F^2}$ is the density of

states of gapless graphene.

3.2.2 Wake effects

The induced number density per unit area of electrons in graphene, n_{gr} , in terms of the local value of the total electric potential, ϕ_{tot} , evaluated at $z=0$, in the form [27]

$$n_{gr} = e\chi(q, \omega)\phi_{tot}(\vec{q}, z, \omega)|_{z=0} \quad (3.35)$$

The total potential $\phi_{tot}(\vec{q}, z, \omega)|_{z=0}$ can be expressed in terms of Fourier transform of the potential $\phi_{ext}(\vec{R}, z, t)$ due to external charge distribution with the density $\rho_{ext}(\vec{R}, z, t)$ as

$$\phi_{tot}(\vec{q}, z, \omega)|_{z=0} = \frac{1}{\epsilon(q, \omega)} \phi_{ext}(\vec{q}, z, \omega)|_{z=0} \quad (3.36)$$

For an external particle Ze moving parallel to gapped graphene sheet, with zero gap between the sheet and substrate, the charge density may be written as

$$\rho_{ext}(\vec{R}, z, t) = Ze\delta(\vec{R} - \vec{v}t)\delta(z - z_0) \quad (3.37)$$

where \vec{v} is the velocity of the particle travelling above the sheet.

The external potential can now be written as

$$\phi_{ext}(\vec{q}, z, \omega)|_{z=0} = \frac{(2\pi)^2 Ze \delta(\omega - \vec{q} \cdot \vec{v})}{q} e^{-qH} \quad (3.38)$$

Substituting these equations in first two equations gives the Fourier transform of the induced number density per unit area of charge carriers in graphene as

$$n_{gr}(\vec{q}, \omega) = 2\pi Z \delta(\omega - \vec{q} \cdot \vec{v}) e^{-qH} \left[1 - \frac{\epsilon_0}{\epsilon(q, \omega)} \right] \quad (3.39)$$

The inverse Fourier transformation in the x-y plane and in time, gives, for a given point charge moving along the x axis with speed v , an expression for induced charge density as follows

$$n_{gr}(x, y, t) = \frac{Z}{\pi^2} \int_0^\infty \int_0^\infty e^{-qH} \text{Re} \left\{ \left[1 - \frac{\epsilon_0}{\epsilon(q, q_x v)} \right] e^{i[q_x(x-vt) + q_y y]} \right\} dq_x dq_y \quad (3.40)$$

$\frac{\epsilon_0}{\epsilon(q, \omega)}$ can be written as

$$\frac{\epsilon_0}{\epsilon(q, \omega)} = \frac{\epsilon_0}{1 - \frac{\omega_p^2}{(\omega + i\eta)^2}} \quad (3.41)$$

$$\therefore 1 - \frac{\epsilon_0}{\epsilon(q, \omega)} = 1 - \frac{\epsilon_0(\omega^2 + i\eta)}{\omega^2 + i\eta - \omega_p^2} \quad (3.42)$$

$$= \frac{-\omega_p^2 + \omega^2(1 - \epsilon_0)}{\omega^2 + i\eta - \omega_p^2} \quad (3.43)$$

using Eq. (3.31) we get,

$$\therefore 1 - \frac{\epsilon_0}{\epsilon(q, \omega)} = \frac{-\omega_p^2 + \omega^2(1 - \epsilon_0)}{\omega^2 + i\eta - \omega_p^2} = \frac{i(-\omega_p^2 + \omega^2(1 - \epsilon_0))}{\pi\omega^2} \delta\left(1 - \frac{\omega_p^2}{\omega^2}\right) \quad (3.44)$$

For gapped graphene $\epsilon_0 = 2.5$

$$1 - \frac{\epsilon_0}{\epsilon(q, \omega)} = i\left(-\frac{\omega_p^2}{\pi\omega^2} - \frac{1.5}{\pi}\right) \delta\left(1 - \frac{\omega_p^2}{\omega^2}\right) \quad (3.45)$$

Let

$$q_x = q\cos\theta, q_y = q\sin\theta, x - vt = r\cos\theta, y = r\sin\theta \quad (3.46)$$

Induced charge density in terms of polar coordinates can be written as

$$n_{gr}(r) = \frac{Z}{\pi^2} \int_0^\infty \int_0^\infty e^{-qH} \text{Re} \left\{ \left[1 - \frac{\epsilon_0}{\epsilon(q, qv\cos\theta)} \right] e^{i[qr\cos^2\theta + qr\sin^2\theta]} \right\} qdq d\theta \quad (3.47)$$

Considering Plasmon-particle contribution to wake effects we have (taking $y = r\sin\theta=0$)

$$n_{gr}(r) = \frac{-z}{\pi^3} \int_0^\infty \int_0^\infty e^{-qH} \left(\frac{\omega_p^2}{(qv \cos \theta)^2} + 1.5 \right) \delta \left(1 - \frac{\omega_p^2}{(qv \cos \theta)^2} \right) \sin(qr \cos^2 \theta) q dq d\theta \quad (3.48)$$

θ integration will lead to the following equation

$$n_{gr}(r) = \frac{1}{2} \int_0^\infty q e^{-qH} \left(\frac{\cos^2 \theta_0}{\cos^2 \theta_0} + 1.5 \right) \eta \left(q - \frac{\lambda^2}{v^2} \right) \sqrt{\frac{\cos^2 \theta_0}{1 - \cos^2 \theta_0}} \delta(\theta - \theta_0) \sin(qr \cos^2 \theta_0) dq \quad (3.49)$$

where $\cos^2 \theta_0 = \frac{\lambda^2}{qv^2}$ and η is the step function

$$n_{gr}(r) = -\frac{Z(2.5)}{2\pi^3} \left(\frac{\lambda}{v} \right) \frac{\partial}{\partial H} \left\{ \int_{\frac{\lambda^2}{v^2}}^\infty e^{-qH} \frac{1}{\sqrt{q - \frac{\lambda^2}{v^2}}} \sin \left(r \frac{\lambda^2}{v^2} \right) dq \right\} \quad (3.50)$$

Numerically the wake effects can be evaluated with the help of following equation

$$n_{gr}(r) = \int_0^{\frac{\lambda^2}{v_f^2}} \int_0^1 \frac{e^{-qH}}{\sqrt{1-z^2}} \left\{ \left(1 - \frac{\epsilon_0 \epsilon_1(q, qvl) \cos[qr l^2]}{[\epsilon_1(q, qvl)]^2 + [\epsilon_2(q, qvl)]^2} \right) - \left(\frac{\epsilon_0 \epsilon_2(q, qvl) \sin[qr l^2]}{[\epsilon_1(q, qvl)]^2 + [\epsilon_2(q, qvl)]^2} \right) \right\} dl dq \quad (3.51)$$

3.3 Results and discussion

3.3.1 Structure Factor and Energy loss

Since $\chi(q, \omega)$ is linearly proportional to q at large q and decreases only like ω^{-1} at large ω in both gapped and gapless graphene, accordingly the structure factor obtained is divergent. In order to improve divergence, we need to add and subtract vacuum polarization inside frequency integral and regularize the structure factor for gapped graphene as well [11]. The Structure Factor before regularization diverges (solid lines) as is the case in SLG . After regularization the structure factor

shows hump and then saturates, though the magnitude after regularization increases (Fig 3.3 & 3.4). Structure factor can be used to obtain basic properties of the system such as energy loss, pair distribution function etc. We implement the calculated structure factor to obtain the numerical results for energy loss. The dynamic and static structure factor has been evaluated for $\alpha = 1.0, 2.0, 4.0$ for $b=0.5$.

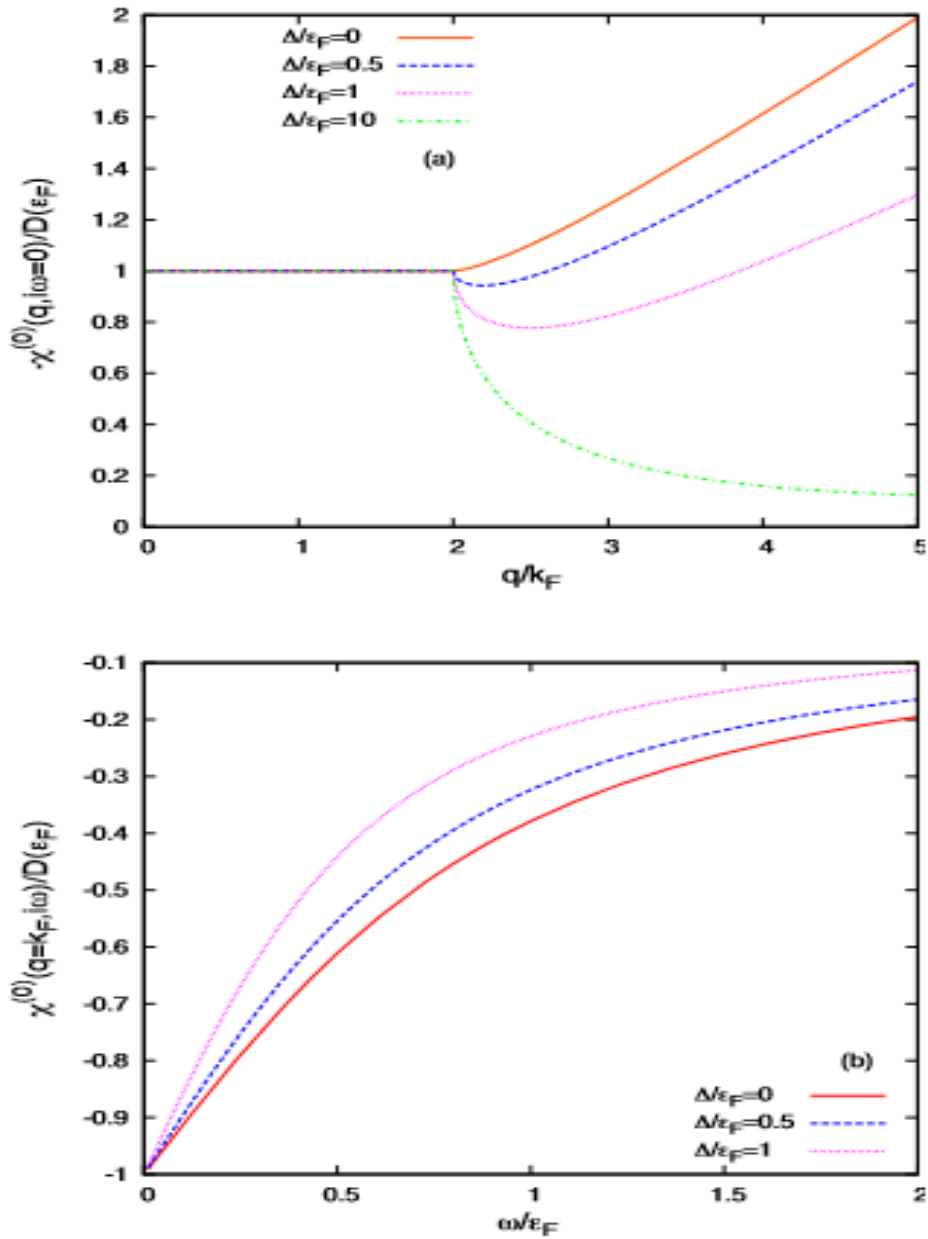


Figure 3.1 Static (above) and dynamic (below) polarization function of gapped graphene [11].

Fig 3.3 displays static structure factor for $\alpha = 2.0$ where solid line clearly diverges for $x > 2.0$, where $x = \frac{q}{k_f}$ is a dimensional less quantity. Regularization makes the curve saturate (Dashed curve) for $x > 2.0$. Same situation can be observed for $\alpha = 4.0$ (Fig 3.4). Fig. 3.1 displays the dynamic structure factor of gapped graphene.

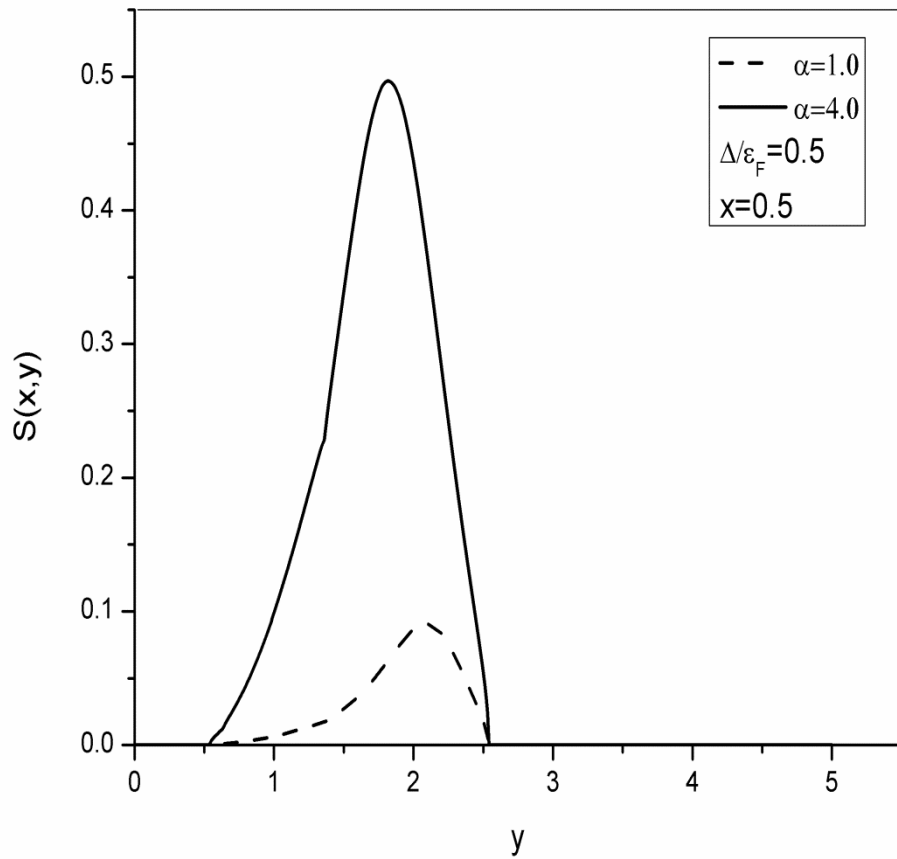


Figure 3.2 Dynamic Structure Factor $S(x, y) \rightarrow y$ for $x=0.5$ and gap $b = \frac{\Delta}{\epsilon_f} = 0.5$ for $\alpha = 1.0, 4.0$

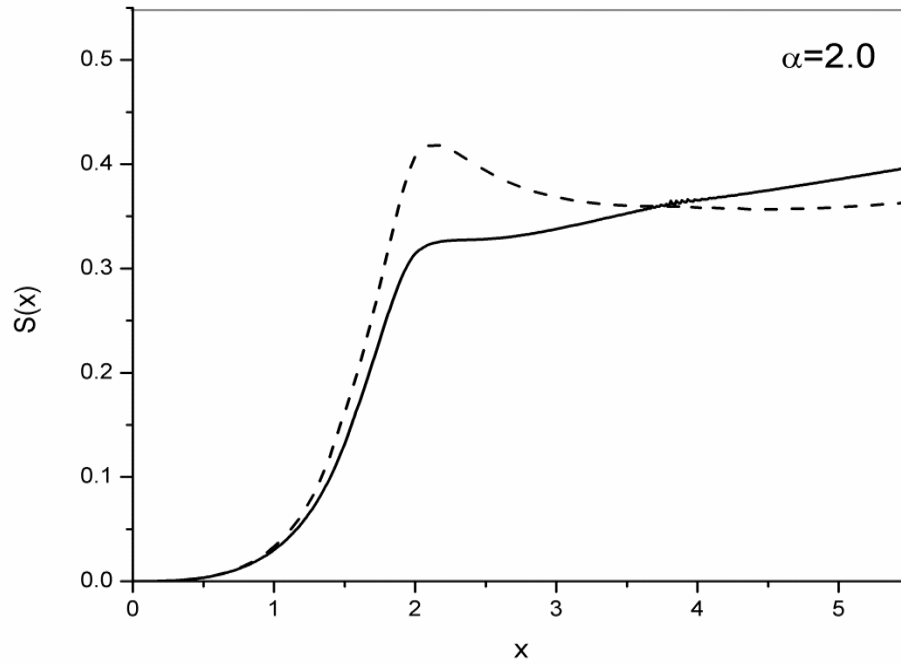


Figure 3.3 Static Structure Factor $S(x) \rightarrow x$ for $\alpha = 2.0$. Solid line (unregularized)
Dashed line (regularized).

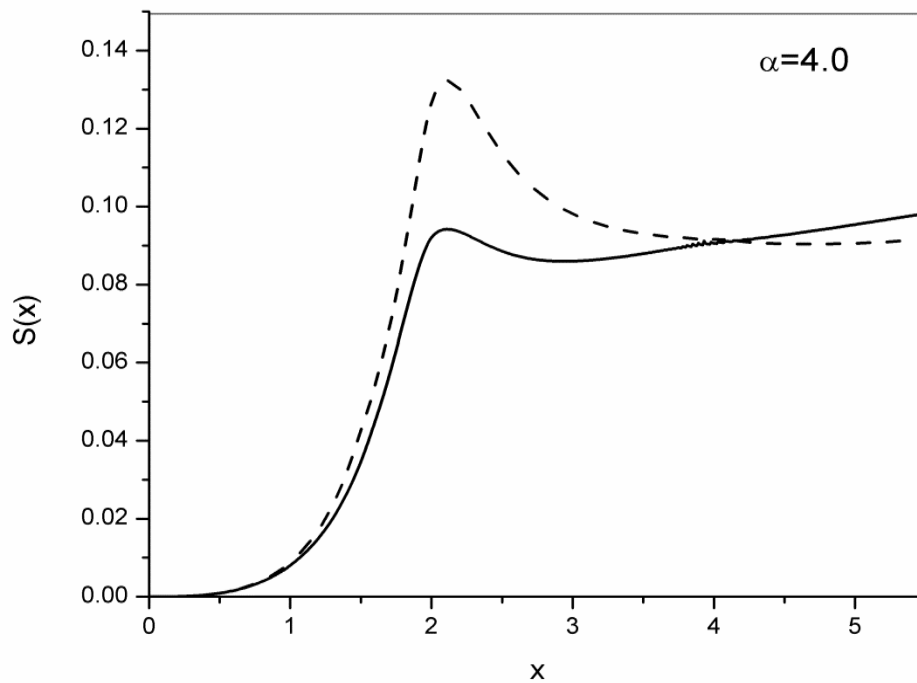


Figure 3.4 Static Structure Factor $S(x) \rightarrow x$ for $\alpha = 4.0$. Solid line (unregularized)
Dashed line (regularized).

The graphs obtained for energy loss of gapped graphene are similar to those obtained for single layer systems. The only difference lies in the magnitude of energy loss.

Analytical results of eq. 3.33 in the limits of high velocity can be expressed in terms of Bessel(Whittaker) functions as,

$$\frac{dW}{dt} = -\frac{Z^2 e^2 \lambda^4}{2\pi\epsilon_0 v^3} \exp\left(\frac{-\lambda^2 H}{v^2}\right) \left[K_0\left(\frac{\lambda^2 H}{v^2}\right) + K_1\left(\frac{\lambda^2 H}{v^2}\right) \right] \quad (3.52)$$

$$\frac{dW}{dt} = \frac{2Z^2 e^2 E_f^2}{\pi\epsilon_0 \hbar^2 v_f} \frac{\alpha^2}{(u)^3 (1+b^2)} \left(e^{-\left(\frac{\alpha x}{(u)^2 \sqrt{1+b^2}}\right)} M + e^{-\left(\frac{\alpha x}{(u)^2 \sqrt{1+b^2}}\right)} N \right) \quad (3.53)$$

$$M = \text{BesselK} \left[0, \frac{\alpha x}{(u)^2 \sqrt{1+b^2}} \right] \quad (3.54)$$

$$N = \text{BesselK} \left[1, \frac{\alpha x}{(u)^2 \sqrt{1+b^2}} \right] \quad (3.55)$$

Where $b \left(= \frac{\Delta}{\epsilon_f} \right)$ is the energy gap in between valence and conduction band of gapped graphene, α is the coupling constant defined in chapter 2 and $u = \frac{v}{v_f}$ ratio of particle velocity to fermi velocity. The results executed here are for $\alpha = 1, 3$ and $b=0.5, 1.5$.

The above results obtained are different for those obtained for SLG [21] by the terms $1/1+b^2$ and $1/\sqrt{1+b^2}$. Thus the energy loss value depends on Gap (b), Coupling constant (α) and ratio of particle velocity to fermi velocity $u = \frac{v}{v_f}$.

As can be seen from figures for fixed α with increase in gap value (b) the energy loss diverges to infinity for $H \rightarrow 0$. In this scenario, with upper cut-off being infinity, with increase in band gap values the energy loss increases with the loss being infinity for $H \rightarrow 0$, irrespective of the values of α and u (Fig 3.5). With increase in the value of α the intensity of energy loss increases. Hence the energy loss is more with coupling getting stronger (Fig 3.6). With increase in the values of u the energy loss reduces as the particle has less time to interact with the system and hence it passes with low energy loss as can be seen from Fig 3.7. In material medium divergence of any quantity is irrelevant. For this an upper cut-off in an integral is required. Energy loss by including full polarization function is obtained using eq. 3.34, which is displayed in fig 3.8. This energy loss comprises of two contribution; particle-hole and plasmons. The results have been already obtained by Godfrey gumbs and group [7].

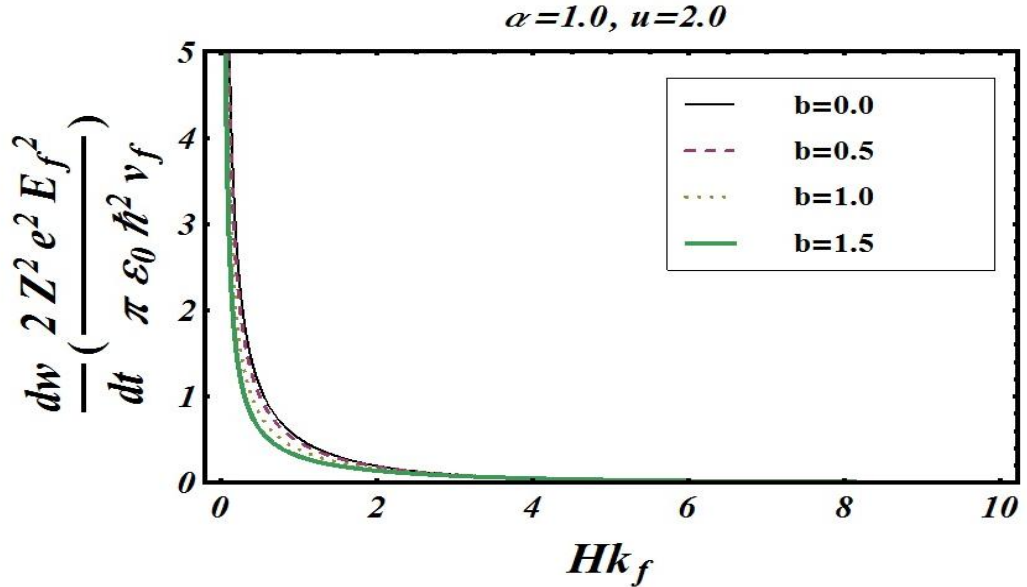


Figure 3.5 Energy Loss dw/dt (in units of $2Z^2 e^2 E_f^2 / \kappa \hbar^2 v_f$) as a function of Hk_f . Solid lines (Thick $\rightarrow \frac{\Delta}{\epsilon_f} = 1.5$; Thin $\rightarrow \frac{\Delta}{\epsilon_f} = 0.5$) $\alpha = 3$; Dotted ($\frac{\Delta}{\epsilon_f} = 1.5$) and Dashed lines ($\frac{\Delta}{\epsilon_f} = 0.5$) for $\alpha = 1$ dotted for the velocity to fermi velocity ratio $\frac{v}{v_f} = 1.0$

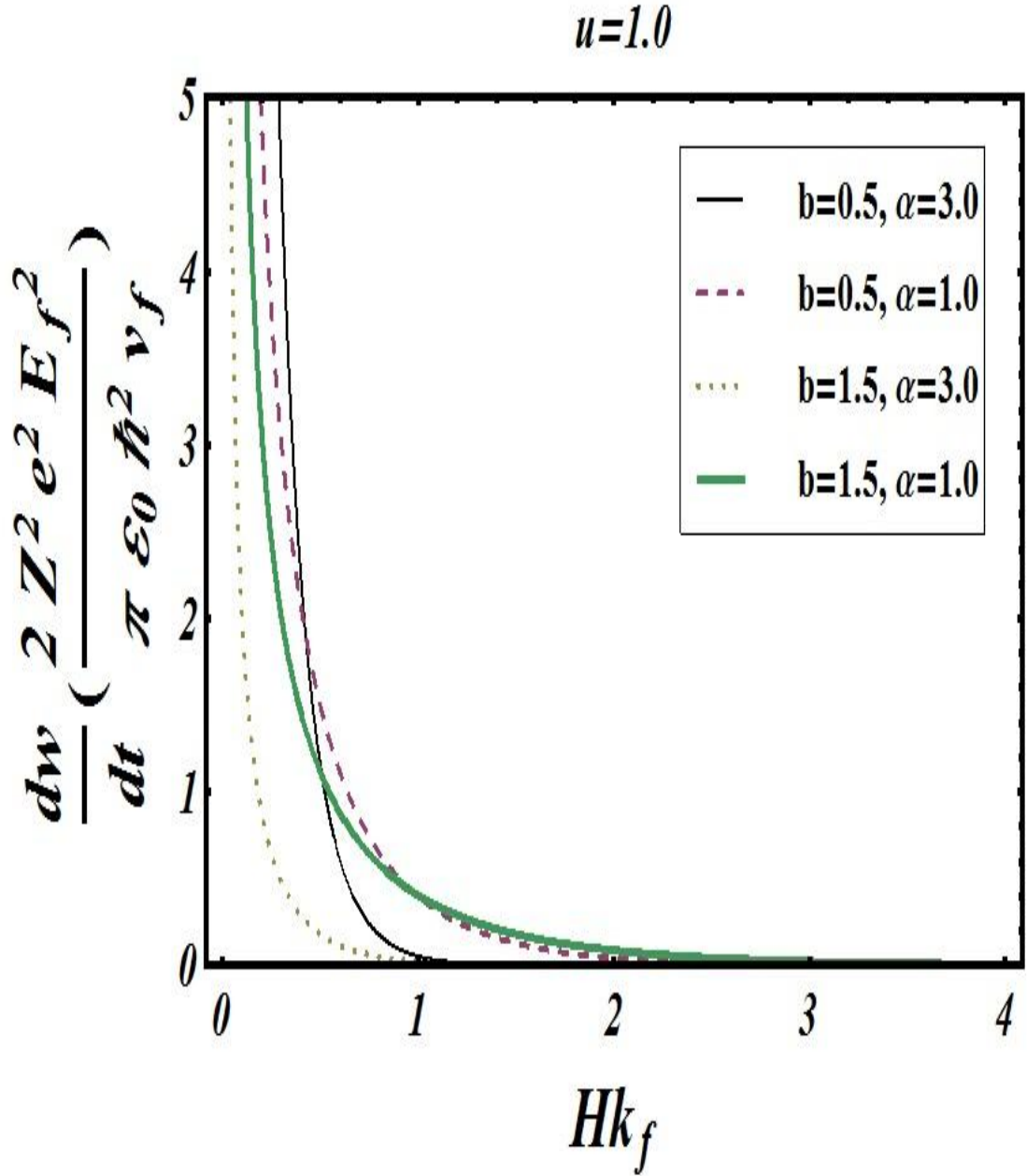


Figure 3.6 Energy Loss dw/dt (in units of $2Z^2 e^2 E_f^2 / \epsilon_0 \hbar^2 v_f \pi$) as a function of Hk_f . Solid lines (Thick $\rightarrow \frac{\Delta}{\epsilon_f} = 1.5$; Thin $\rightarrow \frac{\Delta}{\epsilon_f} = 0.5$) $\alpha = 3$; Dotted ($\frac{\Delta}{\epsilon_f} = 1.5$) and Dashed lines ($\frac{\Delta}{\epsilon_f} = 0.5$) for $\alpha = 1$ dotted for the velocity to fermi velocity ratio $\frac{v}{v_f} = 1.0$

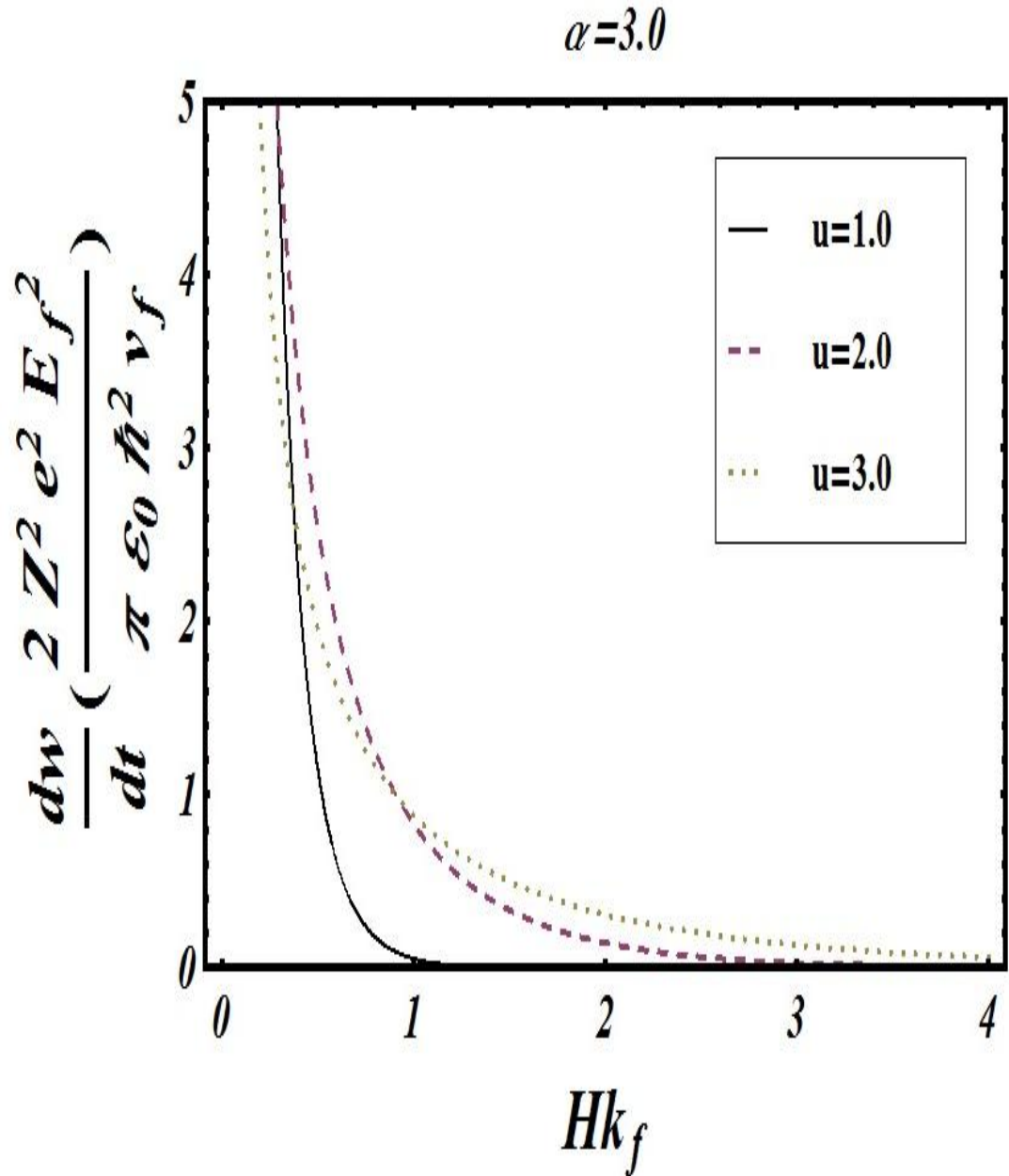


Figure 3.7 Energy Loss dw/dt (in units of $\frac{2Z^2 e^2 E_f^2}{\epsilon_0 \hbar^2 v_f \pi}$) as a function of Hk_f . Solid lines $\frac{v}{v_f} = 1.0$; Dotted $\frac{v}{v_f} = 2.0$; Dashed $\frac{v}{v_f} = 3.0$; $\frac{\Delta}{\epsilon_f} = 0.5$ and $\alpha = 3$

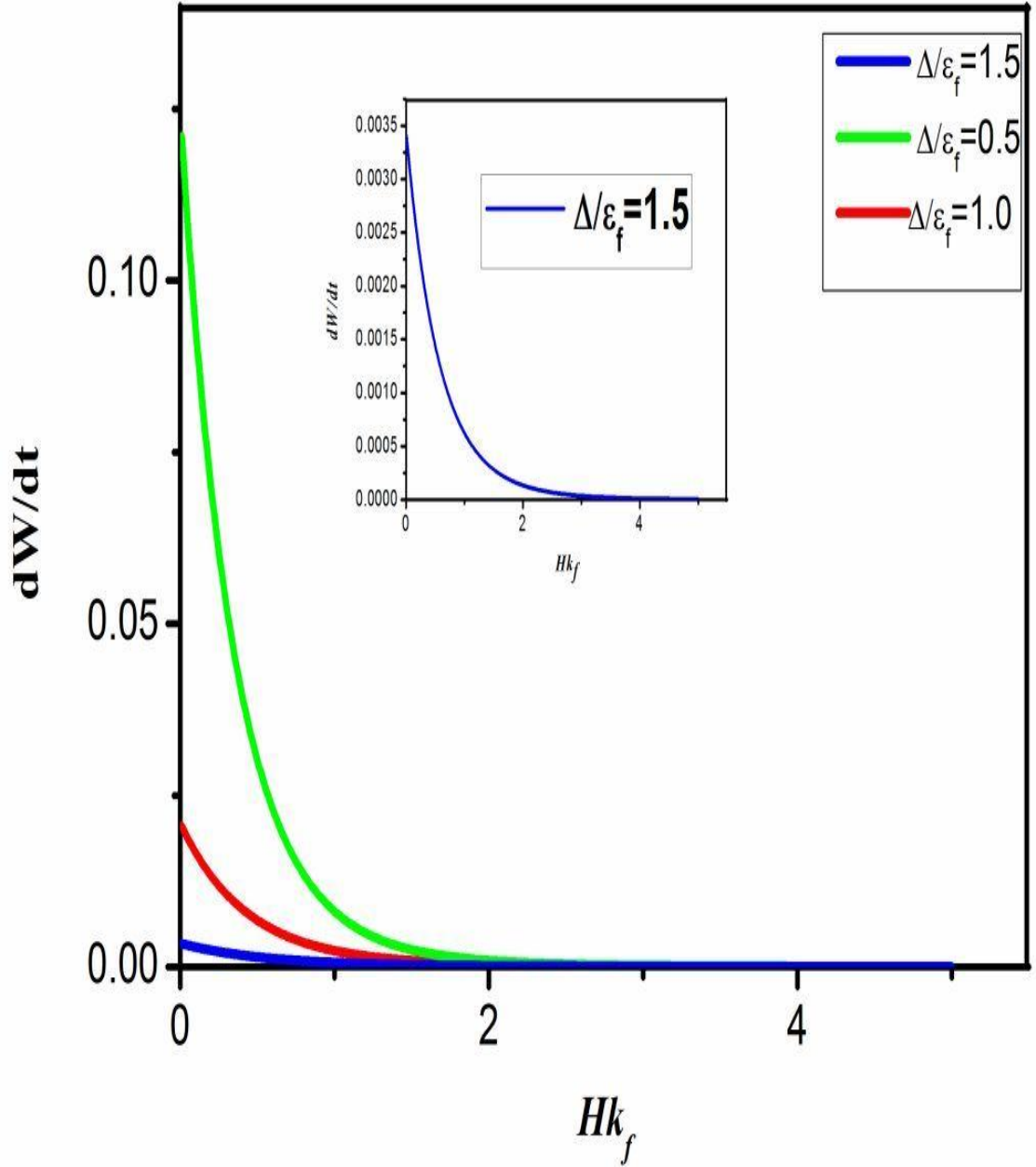


Figure 3.8 Numerical results for energy loss $\frac{dW}{dt} \rightarrow Hk_f$ obtained using eq. 3.34, using full polarization of gapped graphene, for different values of Gap $\frac{\Delta}{\varepsilon_f} = b$. Inset shows $\frac{dW}{dt} \rightarrow Hk_f$ for $\frac{\Delta}{\varepsilon_f} = 1.5$. The $\frac{dW}{dt}$ has been obtained in the units of $\frac{2Z^2 e^2 E_f^2}{\varepsilon_0 \hbar^2 v_f \pi}$.

This eq. 3.33 diverges for high wave number thus it needs a upper cut-off

Setting $q = \frac{\lambda^2}{v^2} x$

$$\frac{dW}{dt} = \frac{Z^2 e^2 \lambda^2}{\epsilon_0 v} \int_{\frac{\lambda^2}{v^2}}^{\frac{\lambda^2}{v_f^2}} dq \sqrt{\left[\frac{q}{\left(q - \frac{\lambda^2}{v^2} \right)} \right]} \quad (3.56)$$

$$\frac{dW}{dt} = \frac{Z^2 e^2 \lambda^4}{\pi \epsilon_0 u^3 v_f^3} \int_1^{u^2} dx \sqrt{\left[\frac{x}{x-1} \right]} \quad (3.57)$$

$$\frac{dW}{dt} = \frac{Z^2 e^2 \lambda^4}{\epsilon_0 v_f^3} \frac{1}{u^3} \left[u \sqrt{u^2 - 1} + \ln \left(u + \sqrt{u^2 - 1} \right) \right] \quad (3.58)$$

$$\frac{dW}{dt} = \frac{2Z^2 e^2 E_f^2}{\pi \epsilon_0 \hbar^2 v_f} \frac{2 \alpha^2}{(u)^3 (1 + b^2)} \left[u \sqrt{u^2 - 1} + \ln \left(u + \sqrt{u^2 - 1} \right) \right] \quad (3.59)$$

Surprisingly considering a cut-off reduces the energy loss with increase in the value of b . As can be seen from figs. 3.9 and 3.10 with increasing u the energy loss is low as the particle has less time to interact with the system. With increase in the value of α the magnitude of energy loss increases.

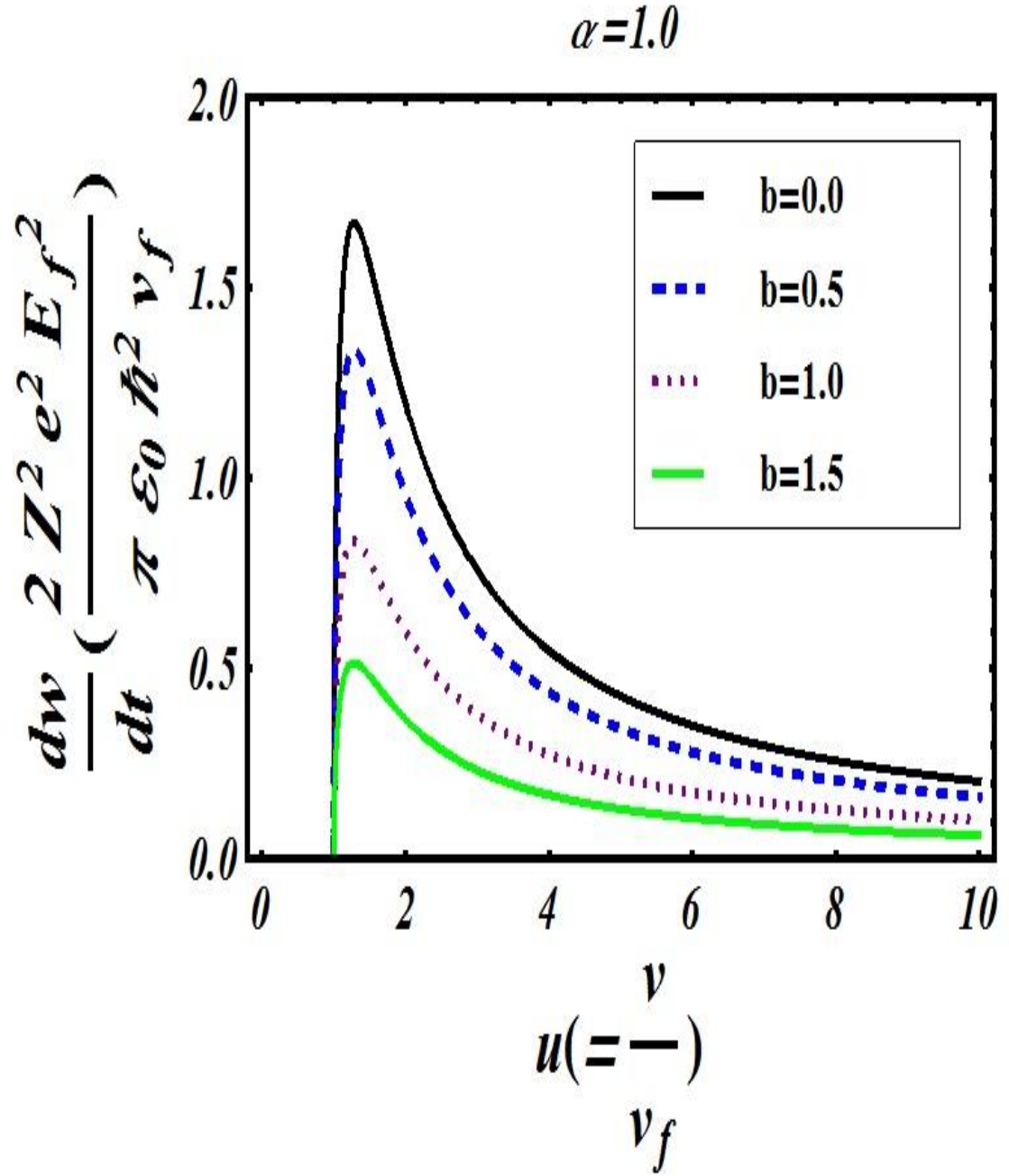


Figure 3.9 Energy Loss dw/dt (in units of $\frac{2Z^2 e^2 E_f^2}{\epsilon_0 \hbar^2 v_f \pi}$) as a function of $\frac{v}{v_f}$ plotted using eq. (3.59), for various values of $b = 0.1, 0.5, 1.0, 1.5$ and $\alpha = 1$

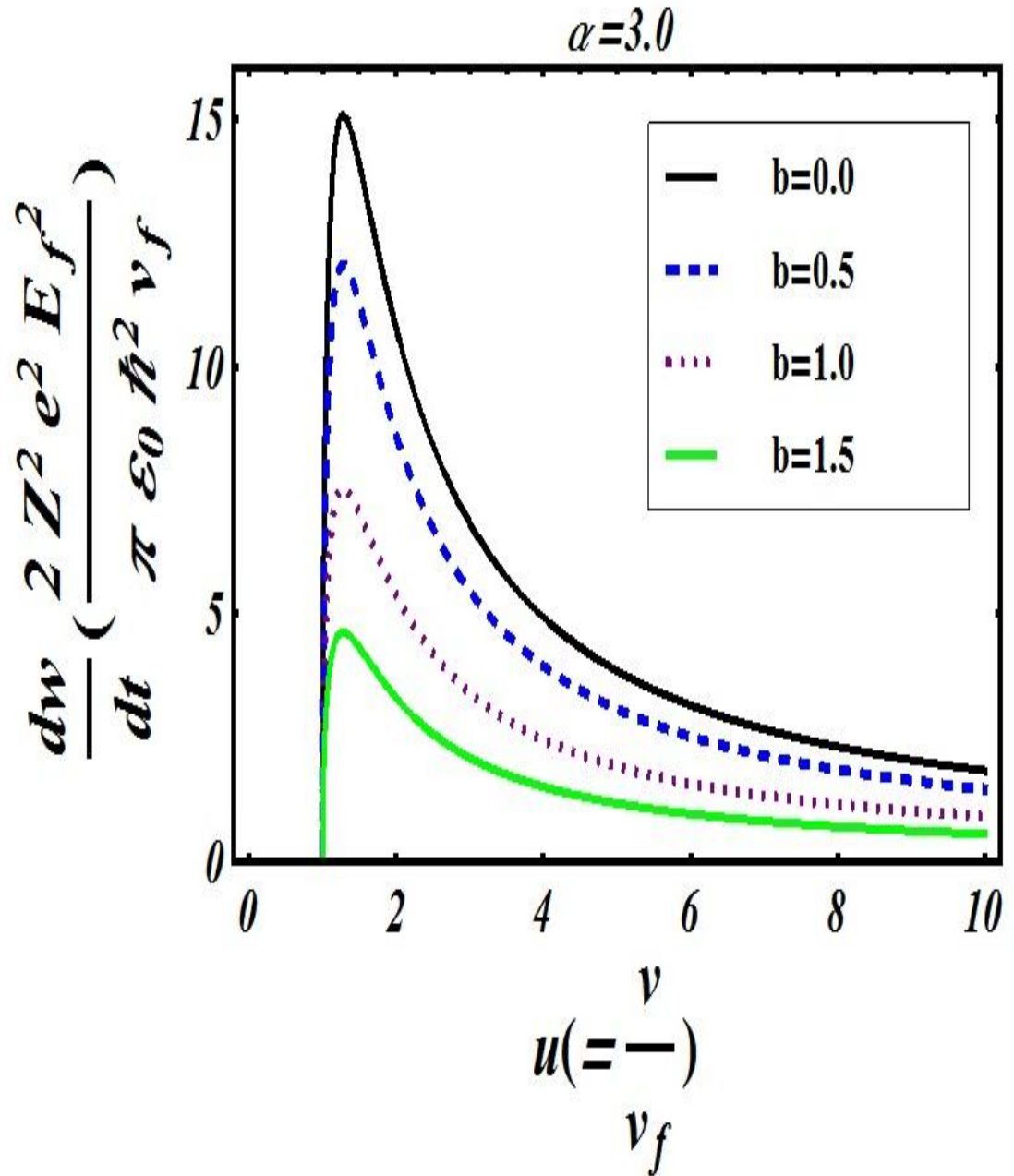


Figure 3.10 Energy Loss dw/dt (in units of $\frac{2Z^2 e^2 E_f^2}{\epsilon_0 \hbar^2 v_f \pi}$) as a function of $\frac{v}{v_f}$ plotted using eq. (3.59), for various values of $b=0.1, 0.5, 1.0, 1.5$ and $\alpha = 3$.

3.3.2 Wake effects

The wake effects arising due to interaction of plasmons with external particle can be obtained with taking into account the plasmons of gapped graphene into calculations.

Wake effects usually arises when particle velocity matches the phase velocity of the system under consideration. Results reported in past has explained the concept numerically for graphene [27] but analytical results were missing. The integration in equation 3.50 yields the following expression.

$$\frac{n_{gr}}{n} = \frac{e^{-Hk_f \frac{\alpha}{\sqrt{1+b^2u^2}}} (Hk_f)^{\frac{3}{4}} \text{Sin} \left[2R \frac{\alpha}{\sqrt{1+b^2u^2}} \right] A}{2^{\frac{1}{4}} \left(\frac{\alpha}{\sqrt{1+b^2u^2}} \right)^{\frac{1}{4}}} \quad (3.60)$$

The final solution of eq. 3.50 comes out in terms of Whittaker function.

$$\begin{aligned} \frac{n_{gr}}{n} = & \frac{3e^{-Hk_f \frac{\alpha}{\sqrt{1+b^2u^2}}} \text{Sin} \left[2R \frac{\alpha}{\sqrt{1+b^2u^2}} \right] A}{2^{\frac{9}{4}} (Hk_f)^{\frac{1}{4}} \left(\frac{\alpha}{\sqrt{1+b^2u^2}} \right)^{\frac{1}{4}}} - \frac{e^{-Hk_f \frac{\alpha}{\sqrt{1+b^2u^2}}} (Hk_f)^{\frac{3}{4}} \frac{\alpha}{\sqrt{1+b^2u^2}} \text{Sin} \left[2R \frac{\alpha}{\sqrt{1+b^2u^2}} \right] A}{2^{\frac{1}{4}} \left(\frac{\alpha}{\sqrt{1+b^2u^2}} \right)^{\frac{1}{4}}} + \\ & \frac{2^{\frac{3}{4}} e^{-Hk_f \frac{\alpha}{\sqrt{1+b^2u^2}}} (Hk_f)^{\frac{3}{4}} \alpha \text{Sin} \left[2R \frac{\alpha}{\sqrt{1+b^2u^2}} \right] \left(\left(\frac{1}{2} - \frac{1}{8Hk_f \frac{\alpha}{\sqrt{1+b^2u^2}}} \right) A - \frac{B}{2Hk_f \frac{\alpha}{\sqrt{1+b^2u^2}}} \right)}{\frac{\alpha}{\sqrt{1+b^2u^2}} \left(\frac{\alpha}{\sqrt{1+b^2u^2}} \right)^{\frac{1}{4}}} \end{aligned} \quad (3.61)$$

$$A = \text{WhittakerW} \left[\frac{1}{4}, -\frac{1}{4}, \frac{2Hk_f \alpha}{\sqrt{1+b^2u^2}} \right] \quad (3.62)$$

$$B = \text{WhittakerW} \left[\frac{5}{4}, -\frac{1}{4}, \frac{2Hk_f\alpha}{\sqrt{1+b^2u^2}} \right] \quad (3.63)$$

where $R = rk_f$

The plot for different b for $u = 1.0, 2.0$ at a fixed distance $Hk_f=0.05$ and coupling constant $\alpha = 1.0$ is displayed in following figures. The value of H is approximately 1\AA and $n = 7.9524 \times 10^{12} \text{cm}^{-2}$. The solution of induced charge density for an infinite upper limit comes out to be in terms of Whittaker function as seen in equ. 3.61. The plot of equ 3.61 is plotted in figs 3.11 and 3.12. There is an increased value of period of oscillation with increase in the value of b . As the value of u increases the number of oscillations reduces as can be compared referring to below two figures.

$$u=2.0, Hk_f=0.05, \alpha=1.0$$

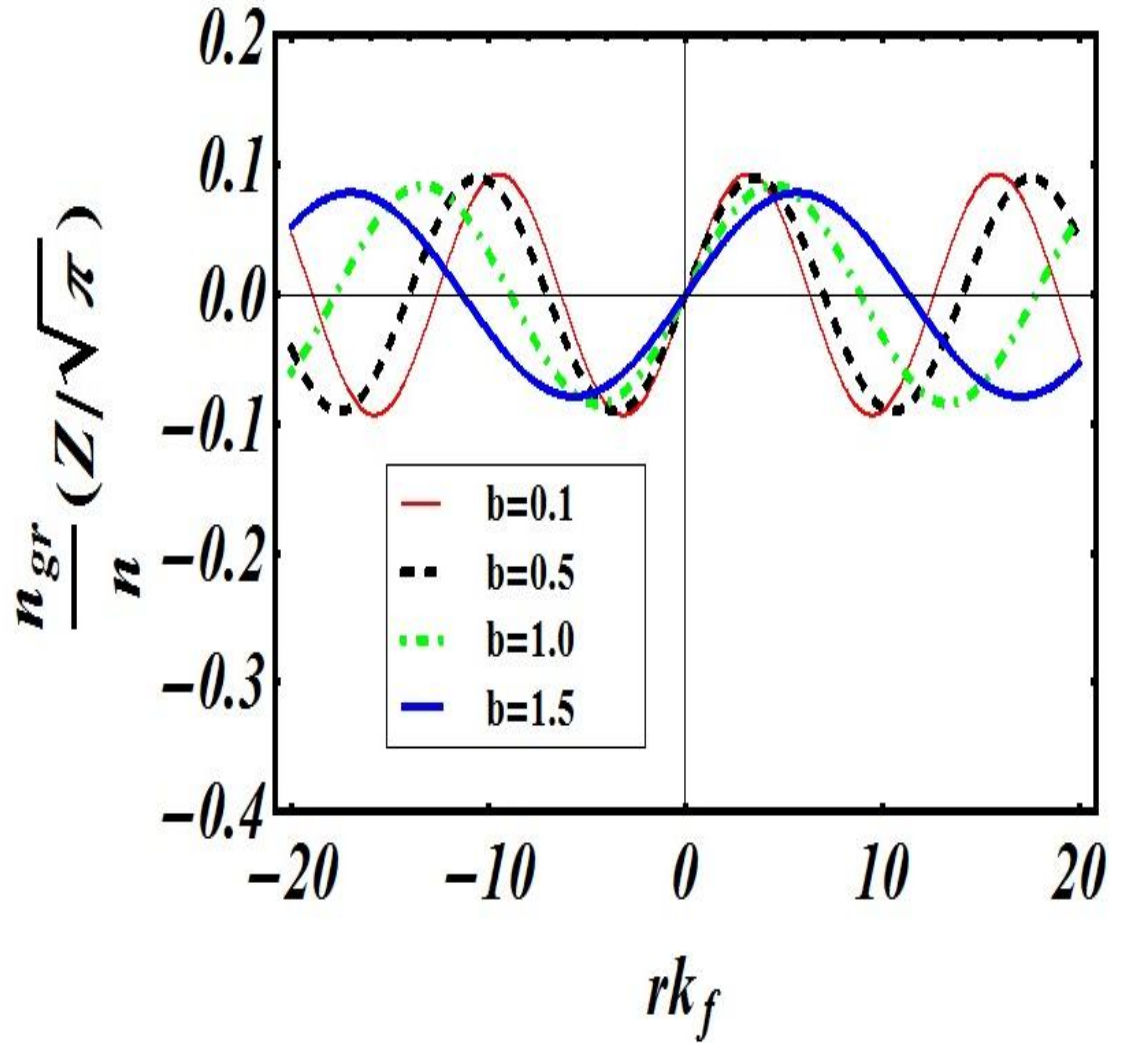


Figure 3.11 Induced charge density $\frac{n_{gr}}{n}$ in the units of $Z\sqrt{\pi}$ Plotted against particle position $rk_f(=R)$ using eq. 3.61, for velocity $\frac{v}{v_f} = 2.0(=u)$; $n = 7.9524 \times 10^{12} \text{cm}^{-2}$ and $\alpha = 1.0$

$$u=1.0, Hk_f=0.05, \alpha=1.0$$

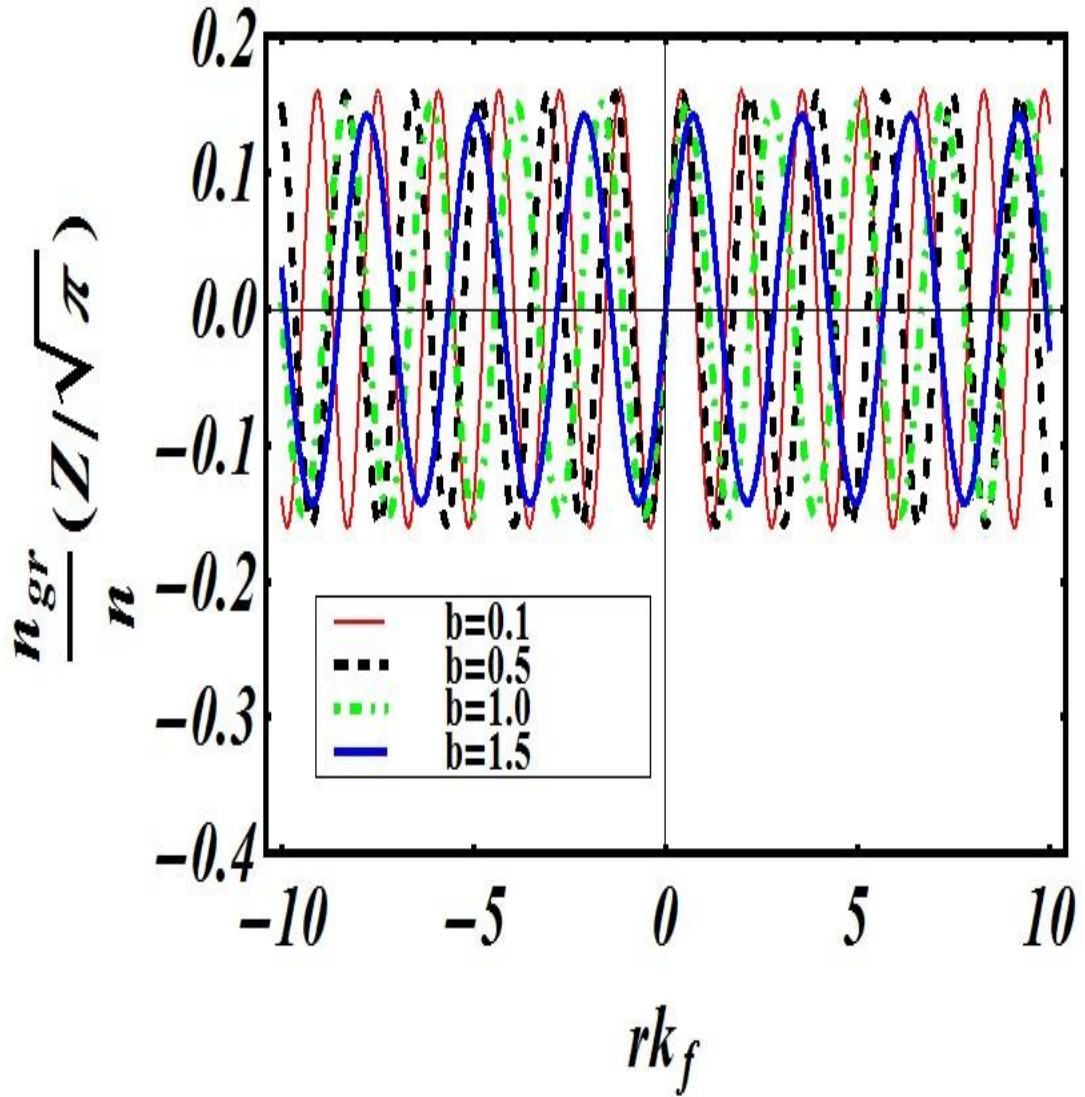


Figure 3.12 Induced charge density $\frac{n_{gr}}{n}$ in the units of $Z\sqrt{\pi}$ Plotted against particle position $rk_f (= R)$ using eq. 3.61, for velocity $\frac{v}{v_f} = 1.0 (= u)$; $n = 7.9524 \times 10^{12} \text{ cm}^{-2}$ and $\alpha = 1.0$

Having a finite upper cut-off limit in equ. 3.50 we have following simplified solution for induced charge density.

$$\begin{aligned}
 \frac{n_{gr}}{n} &= \frac{1}{4\sqrt{2}(Hk_f)^{\frac{3}{2}}\left(\frac{\alpha}{\sqrt{1+b^2u^2}}\right)^{\frac{3}{2}}} e^{-2Hk_f(-2+J)\frac{\alpha}{\sqrt{1+b^2u^2}}} \left(-2\sqrt{2}e^{2Hk_f\frac{\alpha}{\sqrt{1+b^2u^2}}}\sqrt{Hk_f}\sqrt{J}\sqrt{\frac{\alpha}{\sqrt{1+b^2u^2}}} \right. \\
 &+ e^{2Hk_f\frac{\alpha}{\sqrt{1+b^2u^2}}u^2}\sqrt{\pi}\left(1 \right. \\
 &\left. \left. + 4Hk_f\frac{\alpha}{\sqrt{1+b^2u^2}}\right)\text{Erf}\left[\sqrt{2}\sqrt{Hk_f}\sqrt{J}\sqrt{\frac{\alpha}{\sqrt{1+b^2u^2}}}\right]\right)\text{Sin}\left[2R\frac{\alpha}{\sqrt{1+b^2u^2}}\right]
 \end{aligned} \tag{3.64}$$

where $J = -1 + u^2$

Erf is the error function. The cut-off solution is plotted as shown in figures 3.13 to 3.17.

Induced number density exhibits oscillations on both sides of particle position. Such type of behavior has been previously observed in case of carbon nanotubes [28]. With an upper cut-off the magnitude of induced charge density decreases. i.e. the amplitude decreases by introducing an upper cut-off. This amplitude decreases with increase in the value of b and thereby increasing the period of oscillations and hence the number of oscillations decreases for a range of R , irrespective of the values of α, b, n, H and v (fig.3.13 - 3.17). The graphs are obtained for various combination of α, b, n and v . The two values of n being considered are $n = 7.9524 \times 10^{12} \text{cm}^{-2}$ and $n = 7.9524 \times 10^{14} \text{cm}^{-2}$. There is a drastic change in induced charge density with increase in value of α as can be seen

from the figs. 3.13 and 3.14. These changes can be attributed to single particle excitations. With increase in particle speed , u for a fixed α and H , the shape of graph for induced charge density changes to linear form from a trough or crest like shape as seen from fig 3.14.

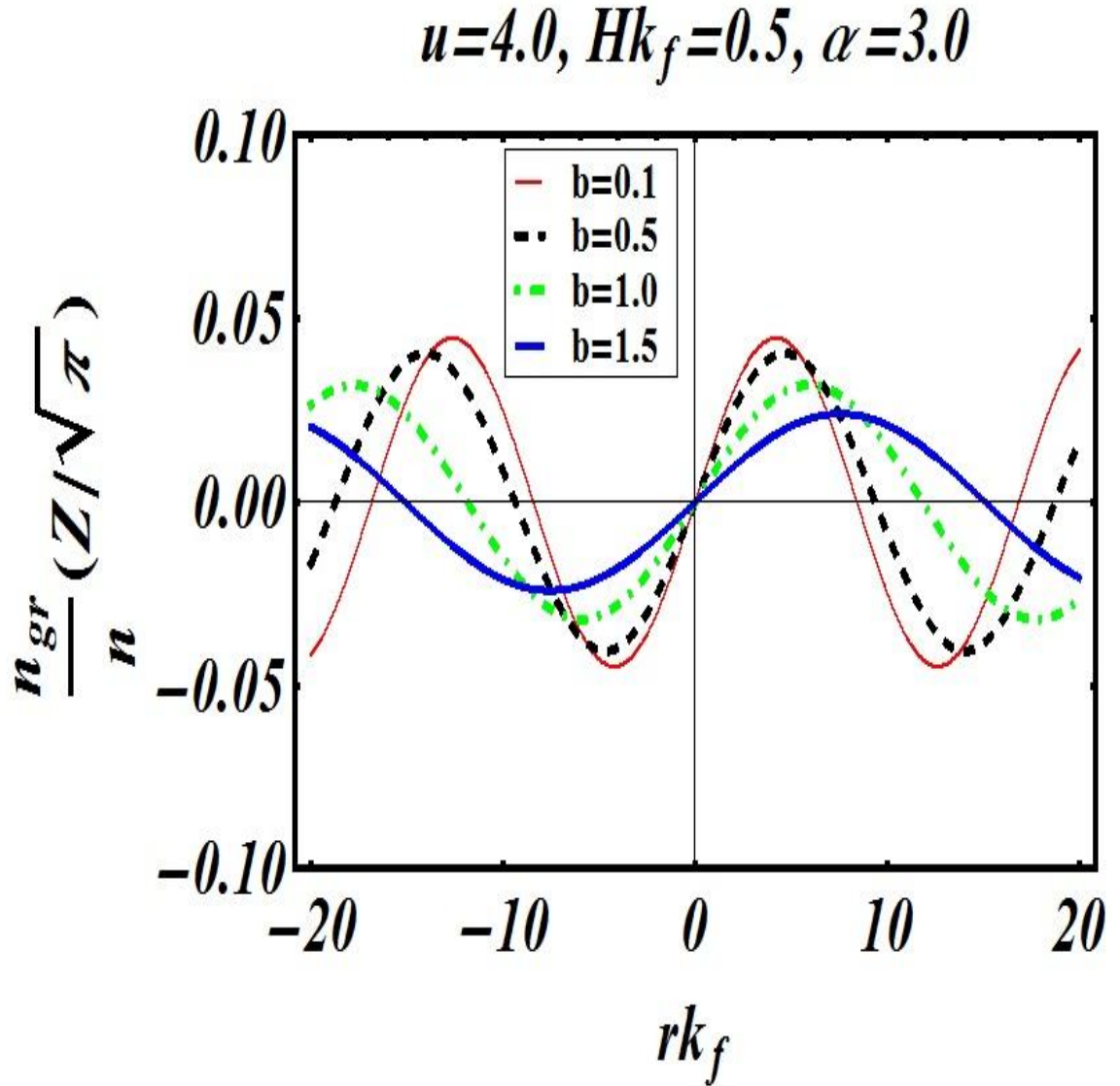


Figure 3.13 Induced charge density $\frac{n_{gr}}{n}$ in the units of $Z\sqrt{\pi}$ Plotted against particle position $rk_f (= R)$ using eq. (3.64), for velocity $u = 4.0$; $n = 7.9524 \times 10^{14} \text{ cm}^{-2}$ and $\alpha = 3.0$

$$u=4.0, Hk_f=0.5, \alpha=1.0$$

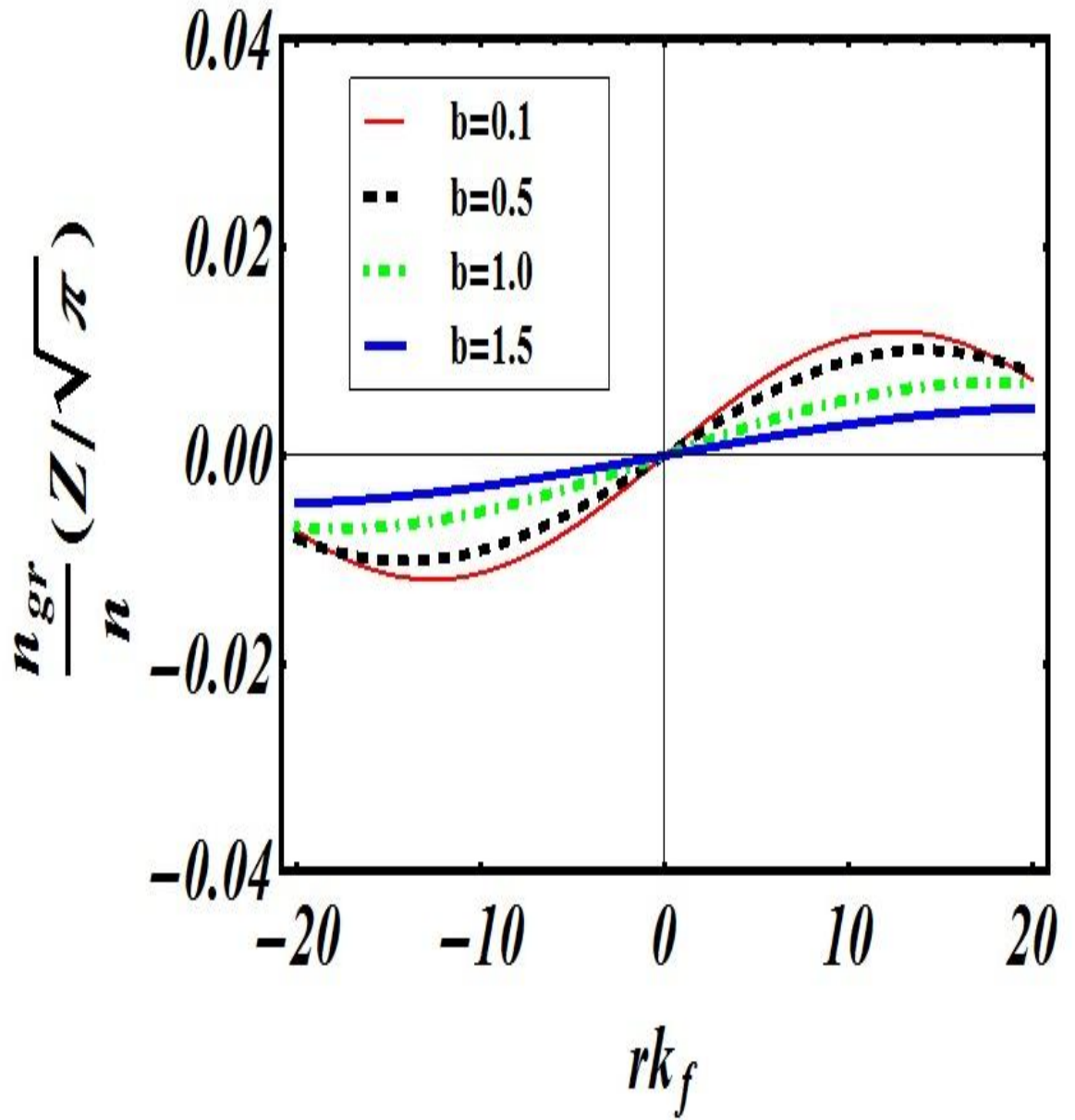


Figure 3.14 Induced charge density $\frac{n_{gr}}{n}$ in the units of $Z\sqrt{\pi}$ Plotted against particle position $rk_f(=R)$ using eq. (3.64), for velocity $u = 4.0$; $n = 7.9524 \times 10^{14} \text{cm}^{-2}$ and $\alpha = 1.0$

$$u=2.0, Hk_f=0.5, \alpha=1.0$$

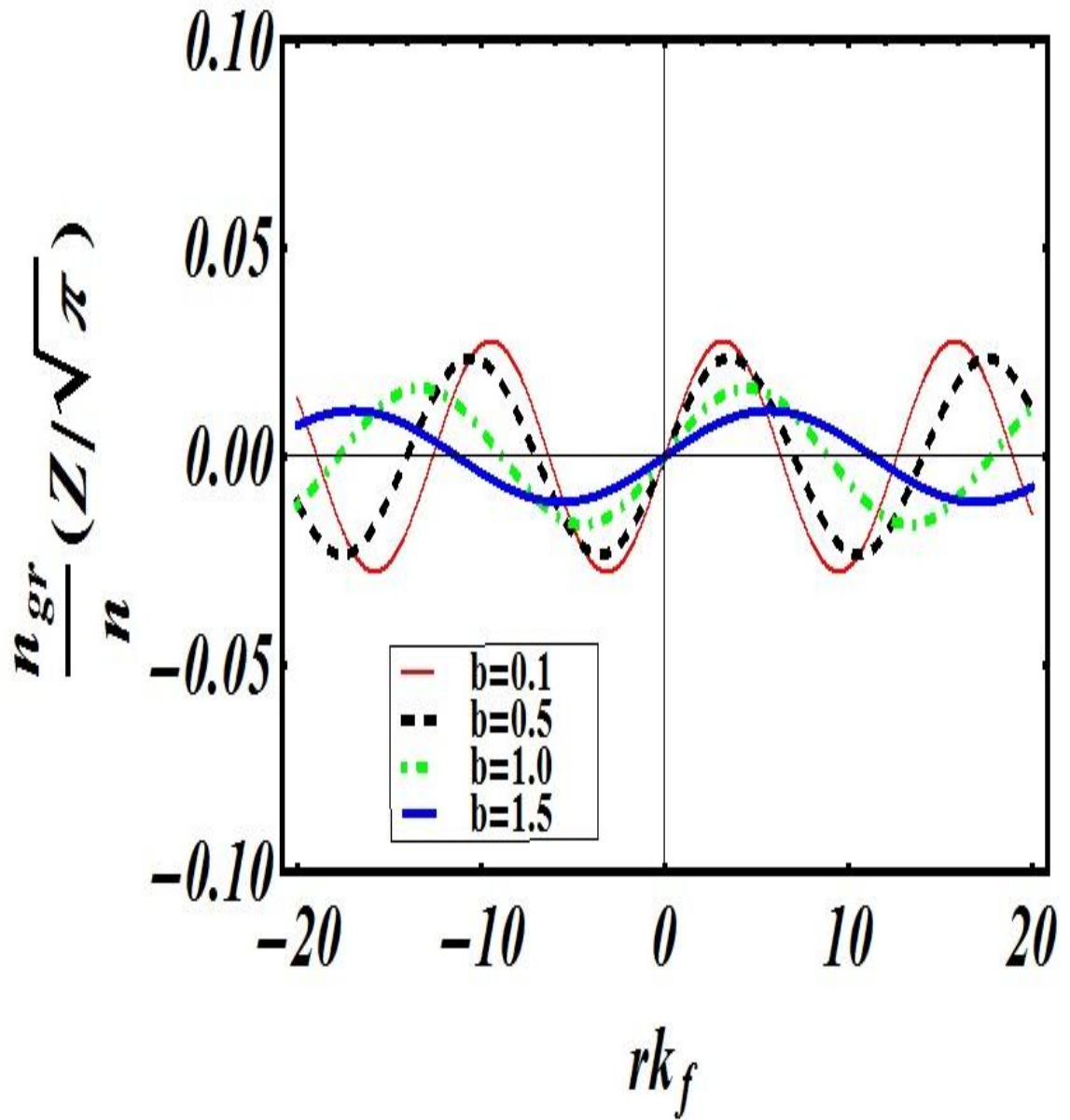


Figure 3.15 Induced charge density $\frac{n_{gr}}{n}$ in the units of $Z\sqrt{\pi}$ Plotted against particle position $rk_f (= R)$ using eq. (3.64), for velocity $u = 2.0$; $n = 7.9524 \times 10^{14} \text{cm}^{-2}$ and $\alpha = 1.0$

$$u=2.0, Hk_f=0.05, \alpha=1.0$$

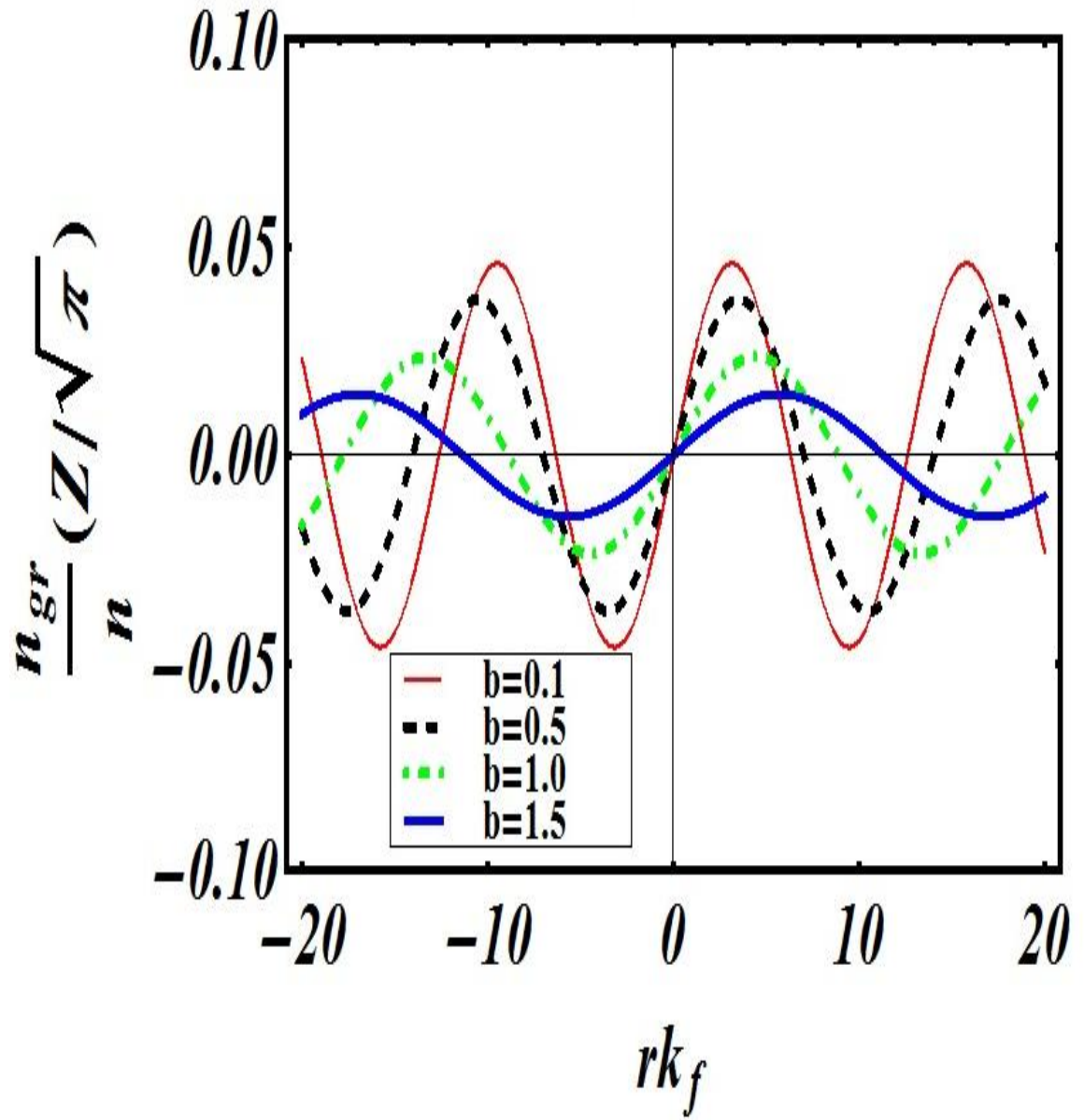


Figure 3.16 Induced charge density $\frac{n_{gr}}{n}$ in the units of $Z\sqrt{\pi}$ Plotted against particle position $rk_f(=R)$ using eq. (3.64), for velocity $u = 2.0$; $n = 7.9524 \times 10^{12} \text{cm}^{-2}$ and $\alpha = 1.0$

Fig. 3.17 displays results of equation 3.51 for n_{gr} for $u=1,4$ and $b=0.5, 1.5$. The results are obtained using full polarization function [4]. The waves are not symmetric with respect to x-axis and their damping can be clearly observed. Unique difference between the analytical and numerical results can be observed because of appearance of Cosine term in the later case (equ (3.51)). There is a finite value of charge density at $rk_f=0.0$, while from fig 3.16 displays zero value for $rk_f=0.0$. This wave pattern on both sides of x-axis was observed for electron gas configuration as well [29]

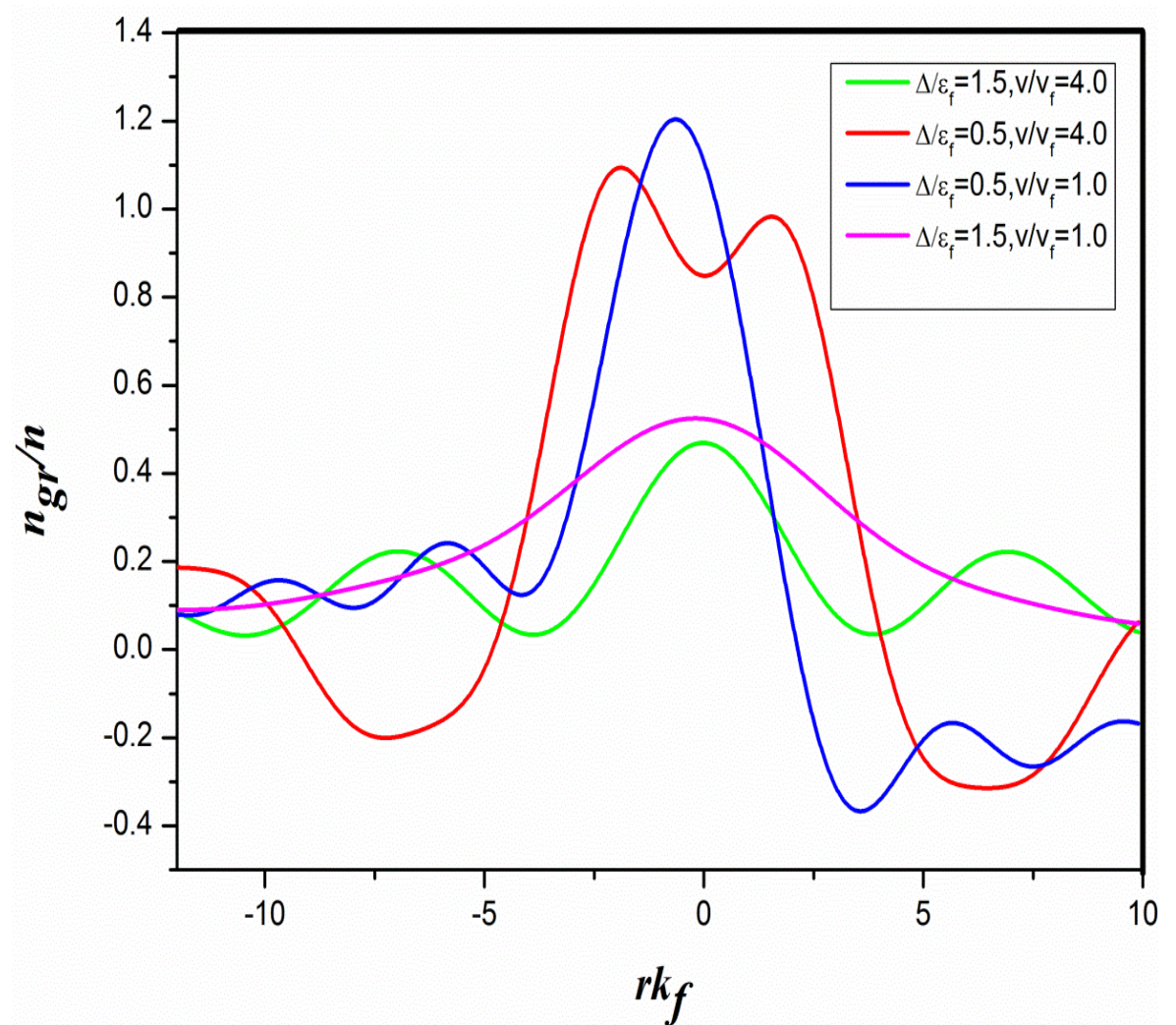


Figure 3.17 Induced charge density $\frac{n_{gr}}{n}$ in the units of $Z\sqrt{\pi}$ Plotted against particle position $rk_f(=R)$ using eq. (3.51), for velocity $u = 1,0.4,0$; $n = 7.9524 \times 10^{14} \text{ cm}^{-2}$ and $\alpha = 1.0$ for gap values $b=0.5$ and 1.5

3.4 References

1. A.H. Castro Neto, F.Guinea, N.M.R. Peres, K.S. Novoselov and A.K.Geim Reviews of Modern Physics Vol 81 109-162, January-March 2009
2. S.Das.Sarma Shaffique Adam E.H.Hwang Enrico Rossi Reviews of Modern Physics, Vol 83, 407- 470, April-June 2011
3. Valeri N.Kotov, Bruno Uchoa, Vitor M. Pereira – Rev. Mod. Phys., Vol 84, 1067-1125, July-September 2012
4. P.K.Pyatkovskiy J.Phys: Cond.Matt. **21** (2009) 025506
5. Oleksiy Roslyak, Godfrey Gumbs and Danhong Huang Journal Of Applied Physics; 109, 11; 113721
6. O.V. Kibis - Phys. Rev. B **81**, 165433 (2010)
7. Godfrey Gumbs, O. Roslyak, Danhong Huang and Antonios Balassis Journal of Modern Optics - 58:21, 1990-1996
8. Fazel Yavari, Christo Kritzinger, Churamani Gaire, Li Song, Hemtej Gulapalli, Theodorian Borca-Tasciuc, Pulickel M. Ajayan and Nikhil Koratkar Small Volume **6**, Issue 22, pages 2535–2538, November 22, 2010
9. Deep Jariwala et.al. Journal of Nanoscience and Nanotechnology Vol. 11, 6621–6641, 2011
10. V.P. Gusynin, S.G. Sharapov, J.P. Carbotte International journal of modern physics b 21 4611 (2007)
11. Alireza Qaiumzadeh and Resa Asgari PRB 79 ,075414 (2009)
12. http://en.wikipedia.org/wiki/Angle-resolved_photoemission_spectroscopy
13. http://en.wikipedia.org/wiki/Electron_energy_loss_spectroscopy
14. <http://www.chembio.uoguelph.ca/educmat/chm729/eels/eels0.htm>
15. T. Eberlein, U. Bangert, R.R. Nair, R. Jones, M. Gass, A. L. Bleloch, K. S. Novoselov, A. Geim, and P. R. Briddon, Phys. Rev. B. 77, 233406 (2008)

16. W. Zhou, S. J. Pennycook, and J.-C. Idrobo, *Ultramicroscopy* **119**,51 (2012)
17. Electron energy-loss spectroscopy in the TEM - R F Egerton *Rep. Prog. Phys.* **72** (2009) 016502
18. I Radovic, L.J. Hadzievski and Z L Miskovic *Phys. Rev. B* **77** 075428 (2008)
19. Kumar S Gupta and Siddhartha Sen *PRB* **78**, 205429 (2008)
20. Wei Zhu, Zhengfei Wang, Qinwei Shi, K.Y.Szeto, Jie Chen, and J.G. Hou *PRB* **79**, 155430 (2009)
21. Vassilios Fessatidis, Norman J.M.Horing, Antonio Balassis *Phys .Lett. A*, **375** 192-198 (2010)
22. E. G. Mishchenko and B. I. Halperin *Phys. Rev. B* **68**, 045317 (2003)
23. Rajdeep Sensarma, E. H. Hwang, and S. Das Sarma *Phys. Rev. B* **82**, 195428 (2010)
24. Charles P. Poole Jr. *encyclopedic dicctonary of condensed matter physics* : Elsevier
25. Kamohara, I. and Ohtsuki, Y. H. , *Phys. Status Solidi B*, **111**: 619–624 (1982).
26. N.J.M.Horing, H.C. Tso and Godfrey Gumbs *PRB* Vol **36** No.3 1588-1594
27. Ivan Radovic, Dusko Borka and Zoran L. Miskovic *Phys. Lett A* **375** (2011) 3720-3725
28. D. J. Mowbray,1 Z. L. Mišković, F. O. Goodman, and You-Nian Wang - *PR B* **70**, 195418 (2004)
29. A.Mazarro, P.M.Echenique and R.H.Ritchie *Phys. Rev. B* **27** No. 7 4117-4128